Silica Nanorattle–Doxorubicin-Anchored Mesenchymal Stem Cells for Tumor-Tropic Therapy

Linlin Li,[†] Yunqian Guan,[‡] Huiyu Liu,[†] Nanjing Hao,[†,§] Tianlong Liu,[†] Xianwei Meng,[†] Changhui Fu,[†] Yanzhen Li,[⊥] Qiulian Qu,[∥] Yingge Zhang,[∥] Shangyi Ji,[⊥] Ling Chen,[‡] Dong Chen,[¶] and Fangqiong Tang[†,*]

[†]Laboratory of Controllable Preparation and Application of Nanomaterials, Technical Institute of Physics and Chemistry, Chinese Academy of Sciences, Beijing 100190, People's Republic of China, [‡]Cell Therapy Center, Beijing Institute of Geriatrics, Xuanwu Hospital, Capital Medical University, Beijing 100053, People's Republic of China, [§]Graduate School of the Chinese Academy of Sciences, Beijing 100049, People's Republic of China, [⊥]Department of Pathology, Sun Yat-Sen Cardiovascular Hospital, Shenzhen 518020, People's Republic of China, [∥]Institute of Pharmacology and Toxicology and Key Laboratory of Nanopharmacology and Nanotoxicology, Beijing Academy of Medical Sciences, Beijing 100850, People's Republic of China, and [¶]Beijing Creative Nanophase Hi-Tech Co., Ltd. China, Beijing 100086, People's Republic of China

ABSTRACT Low targeting efficiency is one of the biggest limitations for nanoparticulate drug delivery system-based cancer therapy. In this study, an efficient approach for tumor-targeted drug delivery was developed with mesenchymal stem cells as the targeting vehicle and a silica nanorattle as the drug carrier. A silica nanorattle–doxorubicin drug delivery system was efficiently anchored to mesenchymal stem cells (MSCs) by specific antibody–antigen recognitions at the cytomembrane interface without any cell preconditioning. Up to 1500 nanoparticles were uploaded to each MSC cell with high cell viability and tumor-tropic ability. The intracellular retention time of the silica nanorattle was no less than 48 h, which is sufficient for cell-directed tumor-tropic delivery. *In vivo* experiments proved that the burdened MSCs can track down the U251 glioma tumor cells more efficiently and deliver doxorubicin with wider distribution and longer retention lifetime in tumor tissues compared with free DOX and silica nanorattle-encapsulated DOX. The increased and prolonged DOX intratumoral distribution further contributed to significantly enhanced tumor-cell apoptosis. This strategy has potential to be developed as a robust and generalizable method for targeted tumor therapy with high efficiency and low systematic toxicity.

KEYWORDS: silica · mesenchymal stem cell · targeting · tumor-tropic therapy · doxorubicin

Tumor-targeted delivery is a great challenge for nanoparticulate drug delivery systems.[1−7] First, most systemically administered nanoparticles circulating along the bloodstream would be rapidly sequestered by the reticuloendothelial system (RES) even with the assistance of tumor-associated enhanced permeation and retention (EPR) effect[8,9] and conjugating with targeting moieties.[10−12] Only a little fraction of nanoparticles could finally accumulate in tumor tissues and specifically effect tumor cells, which would be insufficient to exert optimal therapeutic effect.[13,14] Another limitation impeding targeting efficacy is the stringent vascular endothelial cell barrier and particular solid tumor structure with hypoxic areas, elevated intratumoral interstitial fluid pressure, and dense extracellular matrix.[1,15−17] It results in confined drug penetration and distribution and limited effectiveness. Overcoming these critical physiological barriers imposed by the systematic defense system and abnormal tumor structure for high tumor targeting efficiency and homogeneous intratumoral drug distribution is of great significance for experimental and clinical tumor therapy.

In the past decade, human stem cells, especially neural stem cells (NSCs)[18,19] and mesenchymal stem cells (MSCs),[20−22] have been gene-engineered to track down and destroy malignant cells taking advantage of their tumor-tropic property. Clinical trials using gene-engineered NSCs to treat recurrent high-grade gliomas have been approved in the United States.[23] Attaching nanoparticles to the tumoritropic stem cells is hypothesized to be a promising strategy for actively directing the drug-loaded nanoparticles into tumor.[24] Recently, on the basis of this hypothesis, significant progress has been made by several groups in developing methods to upload nanoparticles to MSCs. Cheng *et al.*[25] designed NeutrAvidin-coated nanoparticles termed as "nanoparticulate patches" on MSCs by biotinylating the plasma membrane. Roger *et al.*[26] discovered that MSCs could internalize polylactic acid nanoparticles (PLA-NPs) and lipid nanocapsules (LNCs) and migrate toward the glioma. Other cell types, including T cell and macrophage, were also used as cell chaperones for targeted delivery of nanoparticles.[27−30] However, up to now, there have no reports about anchoring therapeutic drug-loaded nanoparticles with MSCs for tumor therapy. How to

* Address correspondence to tangfq@mail.ipc.ac.cn.

Received for review June 29, 2011 and accepted August 20, 2011.

Published online August 20, 2011
10.1021/nn202399w

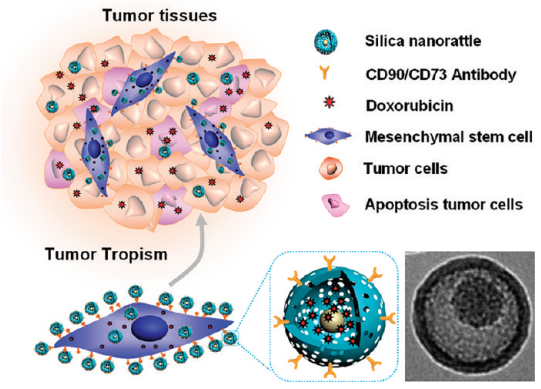

Figure 1. Scheme of silica nanorattle–doxorubicin-anchored mesenchymal stem cells for tumor-tropic therapy.

anchor sufficient therapeutic drug-loaded nanoparticles but with minimum interference of the tumoritropic nature and normal function of MSCs is still a challenge. It is also the most important prerequisite condition for achieving cell-based tumor therapy.

In this study, we first uploaded a doxorubicin–silica nanorattle (SN) drug delivery system (SN-DOX) to MSCs as a "time bomb" for tumor-tropic therapy. SN was used as nanoparticulate drug carriers for their well-defined mesoporous and hollow structure, good compatibility, extraodinarily high drug loading, and sustained drug release properties.[31–34] To upload sufficient drug-loaded nanoparticles to MSCs, SN was bioconjugated with a monoclonal antibody for specifically binding with the MSCs' membrane proteins CD73 and CD90. The uploading of SN-DOX to MSCs had no significant adverse effect on cell proliferation and tropic ability toward U251 human glioma cells. The obtained time bomb of MSC-SN-DOX was able to migrate toward the glioma xenograft, showed more extensive and prolonged drug accumulation in tumor tissues, and further actually increased tumor-cell apoptosis compared with free drug and the drug-loaded silica nanorattle. With extraordinarily high cargo capacity of the silica nanorattle, vigorous tumor-tropic ability of MSCs, and specific nanoparticle–cell association, this strategy prospectively provides an attractive foreground for using MSC-anchored nanoparticulate drug delivery systems for targeted tumor therapy with high efficiency.

RESULTS AND DISCUSSION

In our previous study, we synthesized a silica nanorattle using a facile and scalable selective etching strategy.[31] SN represents a new class of mesoporous silica nanomaterials with a functional core and hollow and mesoporous structure. Attributed to the special structure and good biocompatibility of the silica nanorattle, it was successfully employed as an efficient anticancer drug docetaxel delivery system for cancer therapy.[32–34] SN showed superior performance for

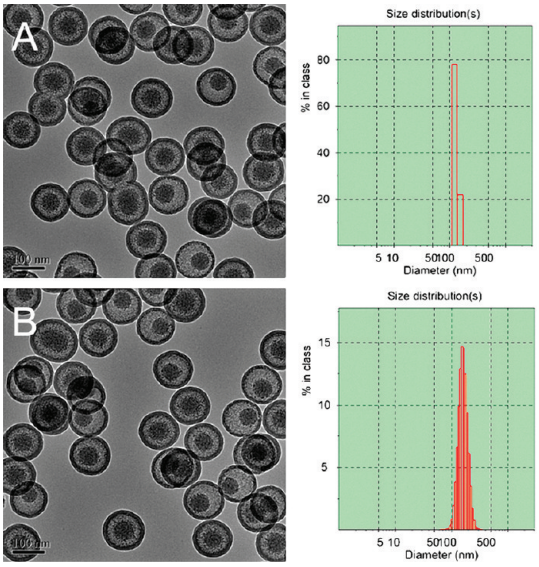

Figure 2. TEM images and size distributions by dynamic light scattering of (A) silica nanorattle and (B) CD90 antibody-bioconjugated silica nanorattle.

increasing the therapeutic efficacy and decreasing the systematic toxicity of the cytotoxic drug. The strategy designed in this work, associating a drug–silica nanorattle delivery system with tumor-tropic MSCs, is schemed in Figure 1. MSC cells, derived from human bone marrow, express specific surface antigens including CD90, CD73, CD105, and CD44 *etc.*[35] These antigens can be used as an anchor to moor the nanoparticles. The silica nanorattle synthesized in our lab has abundant primary amino groups on its particle surface once synthesized. The amino group was carboxylated with glutaric anhydride and then bioconjugated with monoclonal CD73 or CD90 antibody. The antibody-bioconjugated silica nanorattles (SN-Ab) can be specifically uploaded to the MSC cells by antibody–antigen recognitions or a cellular endocytosis process. The laden MSC cells as a time bomb could actively discover and migrate toward solid tumor foci, including the hypoxia region,[36] and release the loaded drug to kill the tumor cells. Not only carcinoma *in situ* but also metastatic tumors and satellite lessions and even single metastatic tumor cells show promise of being tracked down by the MSC-mediated drug delivery system with the powerful tropic ability of MSCs.[18]

Characterization of Antibody-Bioconjugated Silica Nanorattles. SN with a hollow structure and a movable core had an average size of 110 nm determined by TEM (Figure 2A). The hydrodynamic diameter (HD) of the SN determined by dynamic light scattering (DLS) was 125.6 nm. It had a positive ζ-potential of about +35 mV. FITC (fluorescein isothiocyanate)-doped silica nanorattle, which has almost identical size and surface properties with SN,[33] was also prepared for monitoring the nanoparticle. SN was modified with glutaric anhydride to

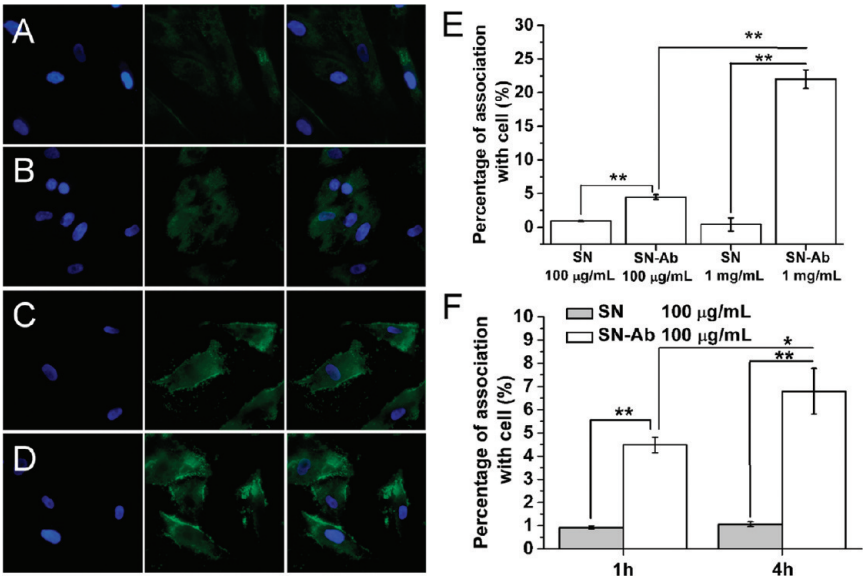

Figure 3. Association of silica nanorattle and CD90 bioconjugated silica nanorattle with MSC cells: (A) 100 μg/mL SN for 1 h, (B) 100 μg/mL SN for 4 h, (C) 100 μg/mL SN-Ab(CD90) for 1 h, (D) 100 μg/mL SN-Ab(CD90) for 4 h. Blue fluorescence shows nuclear staining with DAPI; green fluorescence shows the location of nanoparticles. (E) Nanoparticles with different concentrations were incubated with cells for 1 h, and (F) 100 μg/mL nanoparticles were incubated with cells for 1 and 4 h and then the unassociated nanoparticles were washed off for ICP-OES analysis.

provide surface carboxyl groups. Carboxylated SN was reacted with the amino group of CD73 or CD90 antibody in the presence of *N*-hydroxysulfosuccinimide and 1-ethyl-3-[3-dimethylaminopropyl]carbodiimide hydrochloride (EDC/Sulfo-NHS). After each step of modification, the hydrodynamic diameter and surface charge of the silica nanorattle were characterized, proving the successful surface modification and bioconjugation (Table S1 in Supporting Information). The carboxylated SN showed a negative surface charge of about −20 mV, and the hydrodynamic diameter increased to 130.1 nm. After bioconjugation with CD90 antibody (SN-Ab(CD90)), the hydrodynamic diameter of the nanoparticle further increased to 152.9 nm and the ζ-potential was nearly neutral. There was no obvious morphological change after CD90 antibody bioconjugation (Figure 2B). The antibody-bioconjugated nanoparticle maintained a rather narrow size distribution (Table S1). Similar results were observed with CD73 antibody bioconjugation.

Doxorubicin was loaded on the silica nanorattle with an extraordinarily high loading amount of 18.2%. The doxorubicin showed a pH-sensitive and sustained drug release from the silica nanorattle up to 3 days, with a more rapid drug release rate at pH 4 (close to pH in lysosomes) than at pH 7.4 (pH of blood plasma) (Figure S2). In the initial 1 h, the drug released about 13 and 8% at pH 4 and pH 7.4, respectively. At 88 h, the drug release amount reached 50% at pH 4 but only 11% at pH 7.4. The pH-sensitive drug release profile is consistent with previous reports about DOX release from mesoporous silica nanomaterials,[37,38] which can be attributed to the altered interaction force strength between the silica nanoparticles and drug molecules under different pH values. The high drug loading amount is beneficial for increasing the drug concentration delivered to cancer cells and decreasing the burden of MSCs as nanoparticle vehicles. The pH-sensitive and sustained drug release behaviors are favorable for drug release from nanoparticles into the cytoplasm of cancer cells following endocytosis.

Cellular Interaction and Retention. The MSCs were incubated with SN and SN-Ab(CD90) to compare the cell−nanoparticle interaction with and without antibody conjugation. After 1 or 4 h incubation, 100 μg/mL SN was internalized by MSCs (Figure 3A,B, green fluorescence). The cell association was highly increased for SN-Ab(CD90) of equal concentration (Figure 3C,D), demonstrating that antibody bioconjugation can enhance the association amount of nanoparticles with cells. The result was further quantitatively confirmed by inductively coupled plasma-optical emission spectrometer (ICP-OES) analysis of silicon content in cells. Incubation of 100 μg/mL SN and SN-Ab(CD90) with cells for 1 h can upload 0.92 and 4.48% (calculated to be 1500 nanoparticles per cell) of added nanoparticles to the cells, respectively (Figure 3E). When the concentration was increased to 1 mg/mL, the uploading amount of SN had no detectable increase (0.41%), whereas the uploaded amount for SN-Ab(CD90) was distinctly increase (22%). We speculate that the cellular internalization has been saturated under 100 μg/mL SN. As for the SN-Ab(CD90), the nanoparticle could be more efficiently associated with cells *via* the surface antigen−antibody interaction beside the route of nonspecific cellular uptake, which would be substantially augmented with increasing

nanoparticle concentration. Similarly, increasing the incubation time had no obvious influence on cellular association of SN, but detectable increased association was observed for SN-Ab(CD90) (Figure 3F). After extracellular trypan blue quenching of fluorescence, MSCs had slight decreased fluorescent intensity for both SN and SN-Ab(CD90) interaction (data not shown),[39] demonstrating that the bare and CD90 antibody-bioconjugated nanoparticles could be presented on the cell surface and also be internalized into cells.

Previously, Stephan *et al.* linked lipid nanoparticles with T cells *via* the surface thiols of cells.[28] Cheng *et al.* biotinylated cellular membranes of MSCs for avidin bioconjugation with polystyrene nanoparticles.[25] In these strategies, advanced chemical modifications of the cell or covalent bond forming with cells are needed, which potentially damage native cell functions. For example, Stephan reported that more than 100 nanoparticles per cell would inhibit T cell proliferation.[28] Our strategy uploads nanoparticles using the noncovalent bond between specific antibody–antigen recognition, which does not require any cell preconditioning or chemical modification, ensuring minimal damage to the cells. This strategy also shows advantage of associating as many nanoparticles to cells with high efficiency.

As reported, the stem cells need about 2–4 days to migrate toward and spread through the tumor tissues.[18] The association persistence between nanoparticles and MSCs is of particular importance during the time course of cell homing, ensuring the encapsulated drug is delivered to the tumor sites. After the SN or SN-Ab(CD73) was incubated with MSCs for 1 h, the unbounded nanoparticles were washed off and the cells were cultured for different additional times (6, 24, and 48 h) to detect the nanoparticle retention. After 1 h association, the MSCs had observable green fluorescence for SN (Figure S3A in Supporting Information). After the unbound nanoparticles were washed off and the cells were cultured for an additional 6 h, the fluorescent intensity became weaker (Figure S3B). After an additional 24 h (Figure S3C) and 48 h (Figure S3D), the fluorescent signaling was almost undetectable. This may be attributed to the cellular exocytosis excreting the nanoparticles out of the cells.[40] For the SN-Ab(CD90), the cells showed very strong fluorescence for an additional 6, 24, and 48 h after washing off the unbound nanoparticles (Figure 4). The cells cultured with SN-Ab(CD73) also showed prolonged retention of nanoparticles (Figure S4). With cellular retention time long enough, the loaded drug–nanoparticles could be shipped to the entire tumor tissue to kill the tumor cells. Further study needs to be carried out to confirm the stability of the cell–nanoparticle bomb *in vivo*, where the nanoparticle may be detached passively from MSCs due to shear forces, cell–cell, and cell–substrate interactions in the tissue stroma. Given this possibility, it should anchor a drug delivery system as much as possible to MSCs without compromising key cellular function.

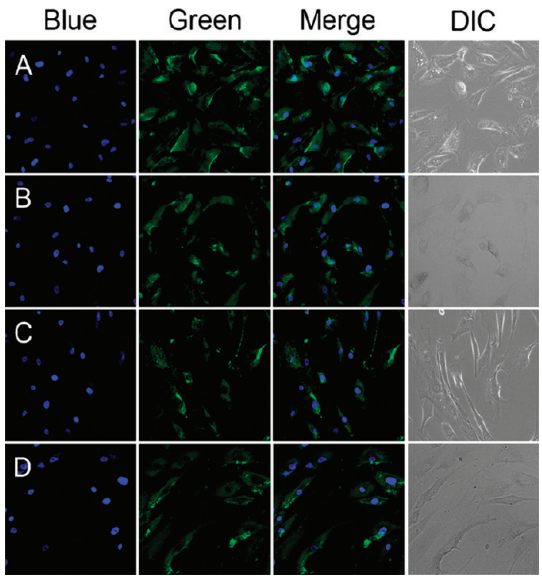

Figure 4. Cellular retention of SN@FITC-Ab(CD90) in MSCs. The MSCs were DAPI stained, incubated with 100 μg/mL SN@FITC-Ab(CD90) for 1 h, cultured for different additional time of (A) 0 h, (B) 6 h, (C) 24 h, (D) 48 h and observed under a fluorescent microscope. Blue fluorescence shows nuclear staining with DAPI, and green fluorescence shows the location of nanoparticles.

Anchoring SN-DOX to MSC with Negligible Toxicity. As mentioned above, the viability and migration ability of MSCs is vitally important for cell-based tropic cancer therapy. Avoiding cellular damage from the nanoparticle-released drug is the key point for successful delivery. After examining cytotoxicity of several chemotherapeutic drugs on MSC at 24 h (Figure S5), we surprisingly found that doxorubicin has negligible adverse effect on MSC viability. The cell viability is higher than 90% even at a high DOX concentration of 16 μg/mL (Figure S5A) by MTT (3-(4,5-dimethylthiazol-2-yl)-2,5-diphenyltetrazolium bromide) assays. We further detected the effect of SN-DOX and SN-Ab(CD90)-DOX on cell viability to examine whether the drug-related cell viability would be changed. The results showed that free drugs (DOX), nanoparticle-encapsulated drugs (SN-DOX), and antibody-bioconjugated nanoparticles (SN-Ab(CD90)-DOX) all had relatively mild adverse effect on cell viability (Figure 5A). The cell viability is higher than 85% at all detected doxorubicin concentrations. We also analyzed the cell cycle and cell apoptosis by propidium iodide (PI) staining. Compared with negative control cells, the cells treated with 25 μg/mL DOX and SN-Ab(CD90)-DOX showed unobvious cell apoptosis (Figure 5B–E). The percentage of cell apoptosis was 1.8% for control, 1.7% for DOX-treated cells, and 4.7% for SN-Ab(CD90)-DOX-treated cells. It is speculated that the MSC cells have drug-resistant ability especially against doxorubicin. For

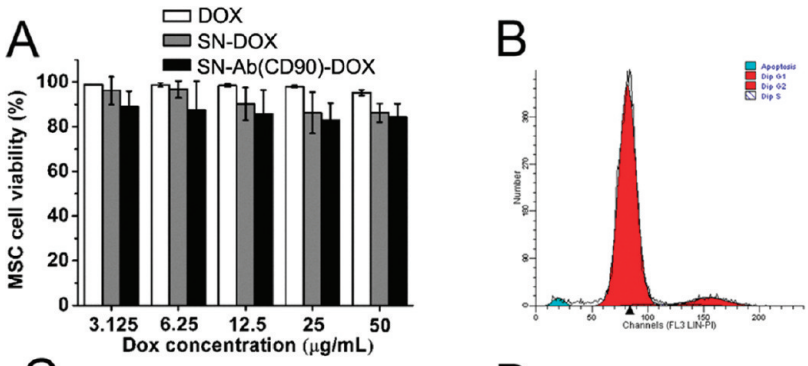

E

	G_0/G_1 (%)	G_2/M (%)	S-phase (%)	Apoptosis (%)	CV(%)
MSC	92.29	5.87	1.84	1.77	9.49
MSC+DOX	78.11	12.62	9.27	1.74	8.02
MSC+SN-Ab(CD90)-DOX	82.97	3.2	13.83	4.65	9.34

Figure 5. Influence of doxorubicin on MSC cell viability. (A) MTT assay showing MSC viability treated with DOX, SN-DOX, and SN-Ab(CD90)-DOX. Cell cycle analysis of (B) MSCs without treatment, (C) DOX, and (D) SN-Ab(CD90)-DOX-treated MSCs, and (E) cell cycle distribution expressed as percentages.

the distribution of cell cycle, G_0/G_1 phase cells in all groups accounted for no less than 75% of all cells. There was an observable but not significant promotion of cell cycle progression from G_0/G_1 to S phase, but this regulation did not show great disturbance to the process of cell proliferation. The absence of cytotoxicity of DOX may be attributed to two reasons. First, doxorubicin was reported to have a cell-cycle-dependent cytotoxicity arresting at G_2/M.[41,42] The lopsided cell cycle distribution, with a large population of cells remaining in G_0/G_1, may result in negligible response to high-concentration DOX. Second, it was reported that many stem cells overexpress ATP binding cassette (ABC) transporters, which play important roles in maintaining their stem-cell state.[43−45] In this study, P-glycoprotein-mediated drug efflux may help for effluxing the drug out of the cells and maintaining the cell in a viable state. These two factors may interdetermine the high viability of cells under high drug concentration, favorable for high cellular association of nanoparticle without compromise of cell viability.

***In Vitro* Tumor Tropism toward U251 Cancer Cells.** To evaluate the tumoritropic property of silica nanorattle−doxorubicin-anchored MSCs, *in vitro* chemotaxis assay was performed using a 24-well transwell chamber. The migration of MSC cells without pretreatment and cells treated with SN, SN-DOX, SN-Ab(CD73), SN-Ab(CD73)-DOX, SN-Ab(CD90), and SN-Ab(CD90)-DOX toward conditioned media (CM) of U251 glioma cells and negative control fibroblasts was measured. Figure 6A−G shows the typical photo of cells that migrate through the membrane pore toward U251 CM. All of the MSCs showed obvious chemotaxis toward the U251 CM compared with fibroblasts (Figure S9). The statistical result (Figure 6H) shows that the MSCs pretreated with SN and SN-DOX had similar migratory capacities, proving that doxorubicin did not influence the migration ability of MSCs. The migratory capacities of MSCs pretreated with SN-Ab(CD73), SN-Ab(CD73)-DOX, SN-Ab(CD90), and SN-Ab(CD90)-DOX were decreased moderately but still adequate for tumor-tropic delivery. It can be attributed that the silica nanorattles attached on the MSC membrane greatly increase after antibody bioconjugation, hampering the MSC deformation to go through the pore of the transwell membrane. During the process of migration, the attached silica nanorattles did not fall off from the MSCs (Figure S10) for both SN with or without antibody bioconjugation. When applied *in vivo*, the environment would be more complicated compared

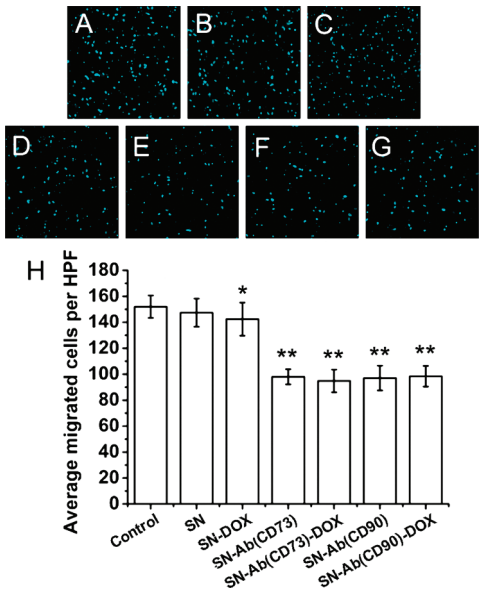

Figure 6. Migration of MSCs toward conditioned media of U251 glioma cells. (A) MSCs without treatment, and MSCs associated with (B) SN, (C) SN-DOX, (D) SN-Ab(CD73), (E) SN-Ab(CD73)-DOX, (F) SN-Ab(CD90), and (G) SN-Ab(CD90)-DOX. (H) Cell amount of migrated MSCs; *$p < 0.05$, **$p < 0.01$, compared with control.

to *in vitro* simulated conditions. During MSC migration confronted with a tumor stroma, it should be further examined whether the particle would be detached due to the shearing forces. It was reported that by carrying 100 nanoparticles, each T cell showed a tendency to inhibit T cell transmigration capacity crossing the endothelial barrier.[28] Here, it is satisfying that 1500 nanoparticles per MSC have acceptable adverse effect on cell viability and migration efficiency.

***In Vivo* Tumor Delivery.** We further examined the *in vivo* cancer homing effect of MSCs carrying doxorubicin-loaded silica nanorattles. Male nude mice with subcutaneous U251 xenografts were intratumorally administered with a single dose of (A) physiological saline, (B) DOX, (C) SN-DOX, and (D) MSC-SN-Ab(CD90)-DOX. The DOX concentration was 5 mg/kg for B–D groups. At 1, 3, and 7 day post-injection, the intratumoral doxorubicin distribution was analyzed by doxorubicin autofluorescence. At 1 day post-injection, the free DOX showed little accumulation in the tumors (Figure S11A), and silica nanorattle-encapsulated DOX penetrated into the solid tumors and accumulated in the nucleus of tumor cells around blood vessels (Figure S11B). Doxorubicin in the MSC-SN-Ab(CD90)-DOX group showed more extensive and dispersed distribution throughout the tumor tissue (Figure S11C). At 3 day post-injection, DOX was only found surrounding the needle insertion point (Figure S12A and data not shown). The distribution of released DOX from SN and the free DOX in MSC-SN-Ab(CD90)-DOX group had no obvious change compared with the results at 1 day post-injection (Figure S12B,C). At 7 day post-injection,

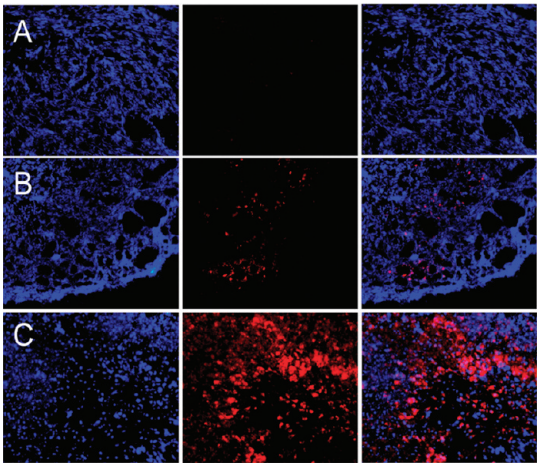

Figure 7. Fluorescent microscopy images of tissue sections 7 days after intratumoral injection of (A) DOX, (B) SN-DOX, and (C) MSC- SN-Ab(CD90)-DOX. Blue fluorescence shows nuclear staining with DAPI, and red fluorescence shows the location of doxorubicin.

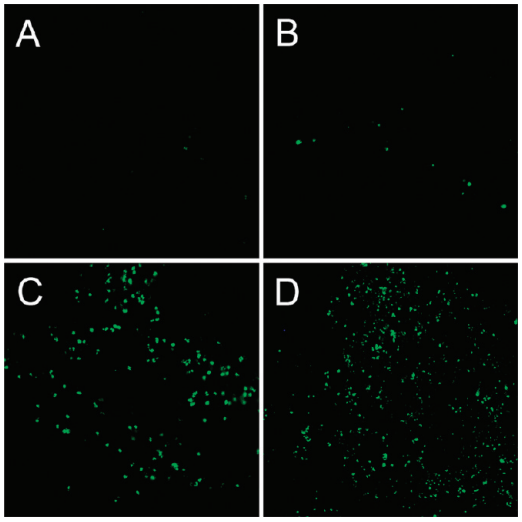

Figure 8. TUNEL staining assay showing apoptosis and cell death by (A) control, (B) DOX, (C) SN-DOX, and (D) MSC-SN-Ab(CD90)-DOX at 7 days after intratumoral injection.

no fluorescence could be observed for free DOX (Figure 7A); the SN-encapsulated doxorubicin showed decreased fluorescence and shrunken distribution area (Figure 7B); and the DOX in MSC-SN-Ab(CD90)-DOX still maintained high level and broad distribution (Figure 7C). Doxorubicin was reported to have low ability for tumor tissue penetration because it has a strong tendency and high level to bind with cellular macromolecues.[14,46] After being encapsulated into the silica nanorattle, the nonspecific binding would be decreased. The increased penetration and accumulation of SN-DOX compared with free DOX is also due to the existence of an EPR effect. After anchoring the SN-DOX drug delivery system to MSCs, the doxorubicin showed wider distribution area and prolonged tumor retention time than SN-DOX due to the tumor-tropic

migration properties of MSCs including targeting the tumor hypoxic area.

Cell apoptosis of tumor tissue was detected using a terminal deoxynucleotidyl transferase dUTP nick end labeling (TUNEL) at 7 day post-injection (Figure 8). For the MSC-SN-Ab(CD90)-DOX group, the possible MSCs apoptosis can be neglected according to the *in vitro* results with negligible MSC cytotoxicity of SN-Ab(CD90)-DOX. Corresponding with the doxorubicin distribution, mice treated with free DOX showed minimal apoptosis among the three treatment groups (Figure 8B); silica nanorattle-encapsulated DOX showed moderate apoptosis (Figure 8C), whereas mice treated with MSC-SN-Ab(CD90)-DOX showed the widest cell apoptosis area (Figure 8D). This result proves that the increased and prolonged doxorubicin distribution with silica nanorattle encapsulation can increase the toxicity to tumor cells. Using MSC to deliver the drug delivery system can actively direct tumor targeting and increase intratumoral distribution and further enhance the tumoral apoptosis and increase the tumor therapy efficiency. Further work is required, and we will further evaluate the *in vivo* cancer therapy efficacy of this strategy.

Cytotoxic drugs have high toxicity to normal tissues, which restricts the dose escalation to obtain an optimal dose for killing cancer cells. Heterogeneous distribution of systemically administered drug also limits the cancer therapy efficacy. With the powerful homing property of MSCs, the drug-loaded nanoparticles have improved tumor targeting with increased drug penetration and more homogeneous intratumor distribution. The therapeutic index would be substantially increased by reducing off-target toxicities and increasing drug concentration at the target sites simultaneously. Furthermore, not only can MSCs find tumor cells but they also can track down islands of tumor cells migrating away from the main tumor mass, which advise a new strategy to track down and kill metastatic cancer. It is also important for therapy of central nervous disease. Even after being injected into the tail vein, the neural stem cells (NSC) were reported to be capable of passing through the blood brain barrier (BBB) and being distributed throughout the intracerebral tumor mass.[18] Although nanoparticles were developed to help transporting across the BBB, the efficiency by passive transport was relatively low.[47] The assembly of a homing cell with a nanoparticulate drug delivery system as a time bomb can be used as a promising and robust candidate to overcome the insurmountable obstacle of an intracranial tumor.

CONCLUSION

The present study demonstrates the design of a time bomb for cancer targeting therapy using the tumortropic property of MSC as a delivery vector and silica nanorattle-encapsulated DOX as a bullet. With specific antibody bioconjugation, the silica nanorattle has increased and prolonged association with MSCs. Compared with free drug and silica nanorattle-encapsulated DOX, the time bomb shows superior advantages in increased and prolonged intratumoral drug distribution and resulting enhanced tumor cell apoptosis. The combination of "stem cell targeting" and "controlled drug delivery" has promised to target and kill all of the tumor cells including the primary and metastasis satellites. This robust and effective strategy provides a promising alternative way for efficient cancer targeting and therapy.

EXPERIMENTAL METHODS

Chemicals. Tetraethyl orthosilicate (TEOS) and *N*,*N*-dimethylformamide (DMF) were obtained from Beijing Chemical Reagents Company (China). *N*-Hydroxysulfosuccinimide (NHS), 1-ethyl-3-[3-dimethylaminopropyl]carbodiimide hydrochloride (EDC), fluorescein isothiocyanate (FITC), and glutaric anhydride were purchased from Sigma. Doxorubicin was purchased from Hafeng United Technology Co. (Beijing). mPEG-SC (methoxy-poly(ethylene glycol)succinimidyl carbonate) (5000 Da) was purchased from Kaizheng Biotechnology Co. (Beijing).

Preparation of Silica Nanorattle and Antibody Bioconjugation. SN and SN@FITC were fabricated *via* a modified Stöber reaction according to our previously reported method.[31] For antibody bioconjugation, 100 mg of SN was reacted with 0.5 mM glutaric anhydride in DMF overnight to get a carboxylated silica nanorattle (SN-COOH). Then, EDC (5 mmol) and Sulfo-NHS (12.5 mmol) were dissolved in a SN-COOH suspension (PBS buffer, pH 5.0). After 20 min, mouse anti-human CD90 mAb (R&D System) or mouse anti-human CD73 mAb (R&D System) was added to this solution, then the pH of the reaction system was adjusted to 7.5. The reaction lasted for 4 h at 4 °C. The antibody-bioconjugated nanoparticles (SN-Ab) were isolated by centrifugation and washing repeatedly at 4 °C.

Morphology of the silica nanorattle and antibody-bioconjugated silica nanorattle was observed with a JEM 2100 transmission electron microscope. The ζ-potential and size distribution were characterized by dynamic light scattering using the Malvern Zetasizer 3000HS.

DOX Loading. To load doxorubicin into the silica nanorattle, the silica nanorattle was dispersed in DOX solution (3.5 mg/mL solved in water) and stirred for 24 h, followed by centrifugation and washing three times with PBS to obtain the drug-loaded SN (SN-DOX). The concentration of DOX was determined by UV/vis spectroscopy measurements at a wavelength of 230 nm (JASCO V570 spectrophotometer). Drug loading amount was calculated according to the equation of drug loading amount (%) = $100 \times W_{DOX}/(W_{SN\text{-}DOX})$, where W_{DOX} is the weight of DOX loaded into the nanorattle and $W_{SN\text{-}DOX}$ is the mass of SN-DOX.

Cell Purification and Culture. Human MSCs were isolated from bone marrow of normal donors as described in previous studies[48,49] and were cultured in regular growth medium consisting of low-glucose Dulbecco's modified Eagle's medium (DMEM) (GIBCO) supplemented with 10 mM L-glutamine, 10% fetal bovine serum (FBS) (Hyclone), penicillin (100 U/mL), and streptomycin (100 μg/mL). Human glioma U251 cells (ATCC) were maintained in high-glucose DMEM, supplemented with 10% FBS, 100 U/mL penicillin, and 100 μg/mL streptomycin. All cultures were kept in an atmosphere of 5% CO_2 and 95% air at 37 °C.

Fluorescent Observation. To observe the association of nanoparticles with MSC cells, the MSC cells were seeded on glass-bottom

dishes (35 mm, MatTek Corporation). A final concentration of 100 μg/mL or 1 mg/mL SN@FITC, SN@FITC-Ab(CD90), or SN@FITC-Ab(CD73) was added to the cells and incubated for different times. The cells were then washed with PBS three times, fixed with 4% paraformaldehyde, and stained with 10 μg/mL DAPI (2-(4-amidinophenyl)-6-indolecarbamidine dihydrochloride, Sigma). Micrographs were taken on a Nikon fluorescence microscope (Nikon Eclipse Ti-S, CCD: Ri1). To observe the cellular retention of the nanoparticle, the MSC cells were seeded on glass-bottom dishes, stained with 10 μg/mL DAPI for 2 h, and then incubated with 100 μg/mL SN@FITC, SN@FITC-Ab(CD90), or SN@FITC-Ab(CD73) for 1 h. The cells were washed with PBS three times and observed by microscope. After observation, DMEM medium was replaced and the cells were put back to the incubator. At 6, 24, and 48 h, the same procedure was followed to observe the retention of nanoparticles in the MSCs.

To quantitatively analyze the association of nanoparticles with MSCs, 10^6 cells were treated with 1 mg/mL and 100 μg/mL SN@FITC and SN@FITC-Ab(CD90) for different times, respectively. The cells were collected and sufficiently washed. The Si content of the cells was measured with inductively coupled plasma-optical emission spectrometry (ICP-OES, VARIAN VISTA-MPX, US).

Cell Proliferation Assays. The cytotoxicity of SN, DOX, SN-DOX, and SN-Ab-DOX on MSCs was evaluated by MTT assay. The cells were seeded at a density of 8000 cell/well on 96-well plates (Costar). After incubating the cells with SN, DOX, and SN-Ab-DOX for 24 h, MTT (3-(4,5-dimethylthiazol-2-yl)-2,5-diphenyltetrazolium bromide, Sigma) (final concentration of 5 mg/mL) was added to each well. After 4 h incubation at 37 °C, colorimetric measurements were performed at 570 nm on a scanning multiwell spectrometer (Multiskan MK3 Thermo labsystems). Data were expressed as mean ± standard deviation (SD) of at least six independent experiments.

Cell Cycle Analysis. Intact, DOX or SN-Ab-DOX-treated MSC cells (1×10^6) were fixed using a solution containing 70% ice cool ethanol in PBS for 24 h at 4 °C. After removing the fixation solution, the cell pellets were incubated with DNA staining solution (40 μg/mL propidium iodide and 100 μg/mL RNase A) for 30 min in the dark. Ten thousand cells per sample were analyzed using flow cytometry (FACSCalibur system, Becton Dickinson).

***In Vitro* Migration.** The cell migration assays were performed using 24-well transwell chambers (8 μm pore size; Corning Inc.); 10^5 MSCs suspended in 200 μL serum-free medium were placed in the upper well of the transwell. The lower well was filled with 600 μL of conditioned media from U251 glioma cells and fibroblasts. The conditioned medium was harvested from the culture medium in which cells mentioned above were incubated for 48 h. After being incubated for 4 h, cells on the transwell membrane were fixed in 4% paraformaldehyde. The fixed membrane was then stained with DAPI for 10 min and washed. For each sample, 10 photos were taken with a 10× objective lens, and the number of stained cells migrating through the membrane pores was counted and averaged.

***In Vivo* Delivery.** Balb/c nude mice (male, 4 week old) were injected subcutaneously in the right axillary region with 0.1 mL cell suspension containing 10^7 U251 cells (ATCC). After tumor size reached to about 200 mm^3, the mice were divided into four groups, minimizing weight and tumor size differences. The mice were intratumorally administered with (A) physiological saline, (B) DOX, (C) SN-DOX, and (D) MSC-SN-Ab(CD90)-DOX. The DOX concentration in groups B−D is 5 mg/kg. MSC-SN-Ab(CD90)-DOX suspension was prepared by incubation of SN-Ab(CD90)-DOX with 10^7 MSC for 1 h and then washed off the unassociated nanoparticles. At 1, 3, and 7 day post-administration, mice were euthanized, and the tumors were peeled off and snap-frozen. Five micrometer cryosections were prepared to measure the distribution of DOX under a fluorescence microscope. Sections of the tumor tissues from each group at 7 days after injection were used for TUNEL staining according to the manufacturer's instructions (Invitrogen, Carlsbad, CA).

Statistical Analysis. The level of significance in all statistical analyses was set at a probability of $*p < 0.05$. Data are presented as mean ± SD. Analysis of variance (ANOVA) and *t* tests were used to analyze the data.

Acknowledgment. The work was financially supported by National Natural Science Foundation of China (Nos. 60736001, 30900349, 30800258) and the National Hi-Tech Research and Development Program (`863' Program) of China (No. 2007AA021803).

Supporting Information Available: Characterization of antibody bioconjugation, drug release profile from silica nanorattle, cellular retention of nanoparticle, MSC viability, detailed information of transmigration, and *in vivo* intratumoral drug distribution are available. This material is available free of charge *via* the Internet at http://pubs.acs.org.

REFERENCES AND NOTES

1. Jain, R. K.; Stylianopoulos, T. Delivering Nanomedicine to Solid Tumors. *Nat. Rev. Clin. Oncol.* **2010**, *7*, 653–664.
2. Sanhai, W. R.; Sakamoto, J. H.; Canady, R.; Ferrari, M. Seven Challenges for Nanomedicine. *Nat. Nanotechnol.* **2008**, *3*, 242–244.
3. Peer, D.; Karp, J. M.; Hong, S.; Farokhzad, O. C.; Margalit, R.; Langer, R. Nanocarriers as an Emerging Platform for Cancer Therapy. *Nat. Nanotechnol.* **2007**, *2*, 751–760.
4. Brannon-Peppas, L.; Blanchette, J. O. Nanoparticle and Targeted Systems for Cancer Therapy. *Adv. Drug Delivery Rev.* **2004**, *56*, 1649–1659.
5. Phillips, M. A.; Gran, M. L.; Peppas, N. A. Targeted Nanodelivery of Drugs and Diagnostics. *Nano Today* **2010**, *5*, 143–159.
6. Wagner, V.; Dullaart, A.; Bock, A.-K.; Zweck, A. The Emerging Nanomedicine Landscape. *Nat. Biotechnol.* **2006**, *24*, 1211–1217.
7. Petros, R. A.; Desimone, J. M. Strategies in the Design of Nanoparticles for Therapeutic Applications. *Nat. Rev. Drug Discovery* **2010**, *9*, 615–627.
8. Torchilin, V. Tumor Delivery of Macromolecular Drugs Based on the EPR Effect. *Adv. Drug Delivery Rev.* **2011**, *63*, 131–135.
9. Maeda, H.; Wu, J.; Sawa, T.; Matsumura, Y.; Hori, K. Tumor Vascular Permeability and the EPR Effect in Macromolecular Therapeutics: A Review. *J. Controlled Release* **2000**, *65*, 271–284.
10. Loo, C.; Lowery, A.; Halas, N.; West, J.; Drezek, R. Immunotargeted Nanoshells for Integrated Cancer Imaging and Therapy. *Nano Lett.* **2005**, *5*, 709–711.
11. Farokhzad, O. C.; Cheng, J. J.; Teply, B. A.; Sherifi, I.; Jon, S. Y.; Kantoff, P. W.; Richie, J. P.; Langer, R. Targeted Nanoparticle-Aptamer Bioconjugates for Cancer Chemotherapy *in Vivo*. *Proc. Natl. Acad. Sci. U.S.A.* **2006**, *103*, 6315–6320.
12. Nasongkla, N.; Shuai, X. T.; Ai, H.; Weinberg, B. D.; Pink, J.; Boothman, D. A.; Gao, J. M. cRGD-Functionalized Polymer Micelles for Targeted Doxorubicin Delivery. *Angew. Chem., Int. Ed.* **2004**, *43*, 6323–6327.
13. Huang, X. H.; Peng, X. H.; Wang, Y. Q.; Wang, Y. X.; Shin, D. M.; El-Sayed, M. A.; Nie, S. M. A Reexamination of Active and Passive Tumor Targeting by Using Rod-Shaped Gold Nanocrystals and Covalently Conjugated Peptide Ligands. *ACS Nano* **2010**, *4*, 5887–5896.
14. Minchinton, A. I.; Tannock, I. F. Drug Penetration in Solid Tumours. *Nat. Rev. Cancer* **2006**, *6*, 583–592.
15. Davis, M. E.; Chen, Z. G.; Shin, D. M. Nanoparticle Therapeutics: An Emerging Treatment Modality for Cancer. *Nat. Rev. Drug Discovery* **2008**, *7*, 771–782.
16. Kim, B. J.; Han, G.; Toley, B. J.; Kim, C.-K.; Rotello, V. M.; Forbes, N. S. Tuning Payload Delivery in Tumour Cylindroids Using Gold Nanoparticles. *Nat. Nanotechnol.* **2010**, *5*, 465–472.
17. Primeau, A. J.; Rendon, A.; Hedley, D.; Lilge, L.; Tannock, I. F. The Distribution of the Anticancer Drug Doxorubicin in Relation to Blood Vessels in Solid Tumors. *Clin. Cancer Res.* **2005**, *11*, 8782–8788.
18. Aboody, K. S.; Brown, A.; Rainov, N. G.; Bower, K. A.; Liu, S.; Yang, W.; Small, J. E.; Herrlinger, U.; Ourednik, V.; Black, P. M.; *et al.* Neural Stem Cells Display Extensive Tropism for

Pathology in Adult Brain: Evidence from Intracranial Gliomas. *Proc. Natl. Acad. Sci. U.S.A.* **2000**, *97*, 12846–12851.
19. Müller, F.-J.; Snyder, E. Y.; Loring, J. F. Gene Therapy: Can Neural Stem Cells Deliver? *Nat Rev. Neurosci.* **2006**, *7*, 75–84.
20. Nakamizo, A.; Marini, F.; Amano, T.; Khan, A.; Studeny, M.; Gumin, J.; Chen, J.; Hentschel, S.; Vecil, G.; Dembinski, J.; *et al.* Human Bone Marrow-Derived Mesenchymal Stem Cells in the Treatment of Gliomas. *Cancer Res.* **2005**, *65*, 3307–3318.
21. Porada, C. D.; Almeida-Porada, G. Mesenchymal Stem Cells as Therapeutics and Vehicles for Gene and Drug Delivery. *Adv. Drug Delivery Rev.* **2010**, *62*, 1156–1166.
22. Kucerova, L.; Altanerova, V.; Matuskova, M.; Tyciakova, S.; Altaner, C. Adipose Tissue-Derived Human Mesenchymal Stem Cells Mediated Prodrug Cancer Gene Therapy. *Cancer Res.* **2007**, *67*, 6304–6313.
23. http://clinicaltrials.gov/ct2/show/NCT01172964.
24. Roger, M.; Clavreul, A.; Venier-Julienne, M.-C.; Passirani, C.; Montero-Menei, C.; Menei, P. The Potential of Combinations of Drug-Loaded Nanoparticle Systems and Adult Stem Cells for Glioma Therapy. *Biomaterials* **2011**, *32*, 2106–2116.
25. Cheng, H.; Kastrup, C. J.; Ramanathan, R.; Siegwart, D. J.; Ma, M. L.; Bogatyrev, S. R.; Xu, Q. B.; Whitehead, K. A.; Langer, R.; Anderson, D. G. Nanoparticulate Cellular Patches for Cell-Mediated Tumoritropic Delivery. *ACS Nano* **2010**, *4*, 625–631.
26. Roger, M.; Clavreul, A.; Venier-Julienne, M.-C.; Passirani, C.; Sindji, L.; Schiller, P.; Montero-Menei, C.; Menei, P. Mesenchymal Stem Cells as Cellular Vehicles for Delivery of Nanoparticles to Brain Tumors. *Biomaterials* **2010**, *31*, 8393–8401.
27. Choi, M.-R.; Stanton-Maxey, K. J.; Stanley, J. K.; Levin, C. S.; Bardhan, R.; Akin, D.; Badve, S.; Sturgis, J.; Robinson, J. P.; Bashir, R.; *et al.* A Cellular Trojan Horse for Delivery of Therapeutic Nanoparticles into Tumors. *Nano Lett.* **2007**, *7*, 3759–3765.
28. Stephan, M. T.; Moon, J. J.; Um, S. H.; Bershteyn, A.; Irvine, D. J. Therapeutic Cell Engineering with Surface-Conjugated Synthetic Nanoparticles. *Nat. Med.* **2010**, *16*, 1035–1041.
29. Kennedy, L. C.; Bear, A. S.; Young, J. K.; Lewinski, N. A.; Kim, J.; Foster, A. E.; Drezek, R. A. T Cells Enhance Gold Nanoparticle Delivery to Tumors *in Vivo*. *Nanoscale Res. Lett.* **2011**, *6*, 283–293.
30. Beduneau, A.; Ma, Z. Y.; Grotepas, C. B.; Kabanov, A.; Rabinow, B. E.; Gong, N.; Mosley, R. L.; Dou, H. Y.; Boska, M. D.; Gendelman, H. E. Facilitated Monocyte-Macrophage Uptake and Tissue Distribution of Superparmagnetic Iron-Oxide Nanoparticles. *PloS One* **2009**, *4*, e4343.
31. Chen, D.; Li, L. L.; Tang, F. Q.; Qi, S. Facile and Scalable Synthesis of Tailored Silica "Nanorattle" Structures. *Adv. Mater.* **2009**, *21*, 3804–3807.
32. Liu, T. L.; Li, L. L.; Teng, X.; Huang, X. L.; Liu, H. Y.; Chen, D.; Ren, J.; He, J. Q.; Tang, F. Q. Single and Repeated Dose Toxicity of Mesoporous Hollow Silica Nanoparticles in Intravenously Exposed Mice. *Biomaterials* **2011**, *32*, 1657–1668.
33. Li, L. L.; Tang, F. Q.; Liu, H. Y.; Liu, T. L.; Hao, N. J.; Chen, D.; Teng, X.; He, J. Q. *In Vivo* Delivery of Silica Nanorattle Encapsulated Docetaxel for Liver Cancer Therapy with Low Toxicity and High Efficacy. *ACS Nano* **2010**, *4*, 6874–6822.
34. Liu, H. Y.; Chen, D.; Li, L. L.; Liu, T. L.; Tan, L. F.; Wu, X. L.; Tang, F. Q. Multifunctional Gold Nanoshells on Silica Nanorattle: A Novel Potential Platform for Combination of Photothermal Therapy and Chemotherapy with Low Systemic Toxicity. *Angew. Chem., Int. Ed.* **2011**, *50*, 891–895.
35. Crisan, M.; Yap, S.; Casteilla, L.; Chen, C.-W.; Corselli, M.; Park, T. S.; Andriolo, G.; Sun, B.; Zheng, B.; Zhang, L.; *et al.* A Perivascular Origin for Mesenchymal Stem Cells in Multiple Human Organs. *Cell Stem Cell* **2008**, *3*, 301–313.
36. Rattigan, Y.; Hsu, J.-M.; Mishra, P. J.; Glod, J.; Banerjee, D. Interleukin 6 Mediated Recruitment of Mesenchymal Stem Cells to the Hypoxic Tumor Milieu. *Exp. Cell Res.* **2010**, *316*, 3417–3424.
37. Chen, Y.; Chen, H. R.; Zhang, S. J.; Chen, F.; Zhang, L. X.; Zhang, J. M.; Zhu, M.; Wu, H. X.; Guo, L. M.; Feng, J. W.; *et al.* Multifunctional Mesoporous Nanoellipsoids for Biological Bimodal Imaging and Magnetically Targeted Delivery of Anticancer Drugs. *Adv. Funct. Mater.* **2011**, *21*, 270–278.
38. Meng, H.; Liong, M.; Xia, T.; Li, Z. X.; Ji, Z. X.; Zink, J. I.; Nel, A. E. Mesoporous Silica Nanoparticles To Deliver Doxorubicin and P-Glycoprotein siRNA To Overcome Drug Resistance in a Cancer Cell Line. *ACS Nano* **2010**, *4*, 4539–4550.
39. Slowing, I. I.; Trewyn, B. G.; Lin, V. S.-Y. Effect of Surface Functionalization of MCM-41-Type Mesoporous Silica Nanoparticles on the Endocytosis by Human Cancer Cells *J. Am. Chem. Soc.* **2006**, *128*, 14792–14793.
40. Slowing, I. I.; Vivero-Escoto, J. L.; Zhao, Y. N.; Kandel, K.; Peeraphatdit, C.; Trewyn, B. G.; Lin, V. S.-Y. Exocytosis of Mesoporous Silica Nanoparticles from Mammalian Cells: From Asymmetric Cell-to-Cell Transfer to Protein Harvesting. *Small* **2011**, *7*, 1526–1532.
41. Zhu, X. L.; Kumar, R.; Mandal, M.; Sharma, N.; Sharma, H. W.; Dhingra, U.; Sokoloskit, J. A.; Hsiao, R.; Narayanan, R. Cell Cycle-Dependent Modulation of Telomerase Activity in Tumor Cells. *Proc. Natl. Acad. Sci. U.S.A.* **1996**, *93*, 6091–6095.
42. Lorenzo, E.; Ruiz-Ruiz, C.; Quesada, A. J.; Hernández, G.; Rodríguez, A.; López-Rivas, A.; Redondo, J. M. Doxorubicin Induces Apoptosis and CD95 Gene Expression in Human Primary Endothelial Cells through a p53-Dependent Mechanism. *J. Biol. Chem.* **2002**, *277*, 10883–10892.
43. Lin, T. T.; Islam, O.; Heese, K. ABC Transporters, Neural Stem Cells and Neurogenesis—A Different Perspective. *Cell Res.* **2006**, *16*, 857–871.
44. Zhou, S.; Schuetz, J. D.; Bunting, K. D.; Colapietro, A.-M.; Sampath, J.; Morris, J. J.; Lagutina, I.; Grosveld, G. C.; Osawa, M.; Nakauchi, H.; *et al.* The ABC Transporter Bcrp1/ABCG2 Is Expressed in a Wide Variety of Stem Cells and Is a Molecular Determinant of the Side-Population Phenotype. *Nat. Med.* **2001**, *7*, 1028–1034.
45. Chaudhary, P. M.; Roninson, I. B. Expression and Activity of P-Glycoprotein, a Multidrug Efflux Pump, in Human Hematopoietic Stem Cells. *Cell* **1991**, *66*, 85–94.
46. Jang, S. H.; Wientjes, M. G.; Lu, D.; Au, J. L.-S. Drug Delivery and Transport to Solid Tumors. *Pharm. Res.* **2003**, *20*, 1337–1350.
47. Béduneau, A.; Saulnier, P.; Benoit, J.-P. Active Targeting of Brain Tumors Using Nanocarriers. *Biomaterials* **2007**, *28*, 4947–4967.
48. Morganstein, D. L.; Wu, P.; Mane, M. R.; Fisk, N. M.; White, R.; Parker, M. G. Human Fetal Mesenchymal Stem Cells Differentiate into Brown and White Adipocytes: A Role for ERRα in Human UCP1 Expression. *Cell Res.* **2010**, *20*, 434–444.
49. Kennea, N. L.; Waddington, S. N.; Chan, J.; O'Donoghue, K.; Yeung, D.; Taylor, D. L.; Al-Allaf, F. A.; Pirianov, G.; Themis, M.; Edwards, A. D.; *et al.* Differentiation of Human Fetal Mesenchymal Stem Cells into Cells with an Oligodendrocyte Phenotype. *Cell Cycle* **2009**, *8*, 1069–1079.